Fractional Fourier Transform Receiver for Modulated Chirp Waveforms

Petrov, N.; Yarovoy, Alexander

DOI
10.1109/TMTT.2022.3222225

Publication date
2022

Document Version
Final published version

Published in
IEEE Transactions on Microwave Theory and Techniques

Fractional Fourier Transform Receiver for Modulated Chirp Waveforms

Nikita Petrov and Alexander G. Yarovoy, *Fellow, IEEE*

***Abstract*— A novel receiver structure for the reception of linearly frequency modulated (LFM) chirps carrying additional narrowband (phase) modulation is proposed. A linear relation between the time delay and the beat frequency shift of the target response in stretch processing is exploited to estimate the target range via correlation of the received signal with the replica in a Fractional Fourier Transform (FrFT) domain. According to numerical simulations, the proposed FrFT receiver demonstrates improved performance and computational efficiency over the state-of-the-art solutions for the moderate-to-large bandwidth of the information-carrying modulation. The receiver was integrated into the waveform-agile radar polarimetric agile radar in S band (PARSAX) and its performance has also been verified experimentally.**

***Index Terms*— Automotive radar, fractional correlation, fractional Fourier transform (FrFT), linearly frequency modulated (LFM), phase-coded frequency modulated continuous wave (FMCW), radar signal processing.**

I. Introduction

A LINEARLY frequency modulated (LFM) waveform has been widely used in various radar applications for decades. The simplicity of the hardware with low requirements on analog to digital converter (ADC) sampling frequency, constant peak-to-average power ratio (PAPR) and good Doppler tolerance are the key advantages of the LFM waveform. These advantages come with the cost of the limited flexibility of LFM signals, crucial for the realization of multiple-input multiple-output (MIMO) radars and interference mitigation between different radars. To associate the received signals with the proper transmit channel, different multiplexing schemes are used in MIMO radars. They imply that the transmitted signals are different in time, frequency, chirp slope or code domains, but at the same time lead to the degradation of radar performance by shortening the unambiguous Doppler velocity, degrading the range resolution, or increasing the sidelobe level [1].

A promising approach to address the aforementioned limitations consists of applying information-carrying modulation to chirps. In that way, the received waveform can be processed after mixing with the reference LFM signal (known as dechirping, deramping, and stretch processing)–preserving all the advantages of the LFM signal mentioned above, and adding to them the ability to discriminate different signals, essential for MIMO beam-forming, interference mitigation between different radars, and realization of joint communication and sensing.

The initial research on applying phase modulation to chirps was carried out in [2] and [3] and some insight into the sensing capabilities of such modulation was given in [4]. A filter-bank receiver structure to deal with phase-modulated frequency modulated continuous wave (FMCW) waveform was proposed in [5] and [6]. Therein the authors noticed that the received signal after dechirping has a time delay and the beat frequency shift proportional to the range of the target. To consider these two effects together, the authors proposed the compensated stretch processing [5], [6], which takes both these effects into account. The implementation of the compensated stretch processing requires applying a filter bank for all ranges of interest. Therefore it has the computational complexity of digital Fourier transform (DFT) $\mathcal{O}(N^2)$, where N is the number of samples per chirp at f_s. That is significantly larger than that of the standard dechirping realized via the fast Fourier transform (FFT): $\mathcal{O}(N \log_2(N))$. Thus, the high computational complexity of the compensated stretch processing makes challenging its realization on low-cost FMCW radar applications, e.g., an automotive radar chip.

The state-of-the-art approaches to process phase-modulated FMCW waveforms [7], [8], [9], [10] use the group delay filter in the receiver to align the responses at all range cells before decoding, followed by FFT for range extraction. The original idea of such delay compensation comes from the correction of non-linearity of chirp slope for stretch processing, e.g., [11], [12], [13]. This receiver design, derived with an assumption of a narrowband deviation of the signal from the LFM, significantly degrades for long codes (modulation signals with the bandwidth comparable to the beat signal ADC sampling frequency), which are of the main interest in applications mentioned above. An appropriate predistortion of the transmit signal to compensate for this effect has been proposed [14], [15], which, however, leads to an increase in the PAPR of the transmitted signal, undesirable for the transmission chain.

A conceptually similar approach is proposed in [16] with application to chirps modulated by an orthogonal frequency division multiplexing (OFDM) waveform. Instead of the group

Manuscript received 15 March 2022; revised 1 June 2022; accepted 5 August 2022. Date of publication 29 November 2022; date of current version 7 February 2023. *(Corresponding author: Nikita Petrov.)*

The authors are with the Microwave Sensing, Signals and Systems (MS3), Delft University of Technology, 2628 CD Delft, The Netherlands (e-mail: N.Petrov@tudelft.nl; A.Yarovoy@tudelft.nl).

Color versions of one or more figures in this article are available at https://doi.org/10.1109/TMTT.2022.3222225.

Digital Object Identifier 10.1109/TMTT.2022.3222225

delay filter, they propose a certain rearrangement of the OFDM sub-carriers to realize a symbol-canceling receiver. This, however, imposes multiple constraints on the selection of the waveform parameters.

In this article, we propose a novel receiver design for modulated LFM signals, which demonstrates the ability to recover the range profile accurately, similar to the compensated stretch processing, and does so in the computational complexity of FFT. To do that, we present in Section II-A the signal model and derive the matched filter receiver, which coincides with the compensated stretch processing [5], [6]. It is further shown that due to the linear relation between the time delay and the beat frequency, the matched filter can be realized via the fractional correlation [17], [18], which can be computed efficiently using the fractional Fourier transform (FrFT) with the computational load of FFT [18], [19]. Consequently, in Section III we propose a received based on fractional correlation. The performance of the proposed receiver is compared to the other state-of-the-art solutions through numerical simulations in Section IV and via processing of measured radar data in Section V. Finally, the conclusions are drawn in Section VI.

II. Signal Model and Matched Filter Receiver

A. Signal Model

Assume that the radar transmits a wideband LFM chirp modulated with a narrowband modulation signal $m(t)$

$$s_t(t) = m(t)e^{-j2\pi\left(f_c t+\frac{\beta t^2}{2}\right)}, \quad t \in [0, T] \tag{1}$$

where f_c stands for the carrier frequency of the radar, $\beta = B/T$ is the chirp rate, B and T are the bandwidth of the duration of the chirp, respectively. Moreover, we assume that the bandwidth of $m(t)$ is much smaller than that of the chirp $B_m \ll B$.

Signal (1) impinges on a target at a range r_0 moving with a constant radial velocity v_0 toward or away from the radar. The reflected signal is received by the radar with a time delay

$$\tau_0(t) = \frac{2}{c}(r_0 + v_0 t) = \tau_0 + \frac{2v_0}{c}t \tag{2}$$

attenuated proportionally to the target radar cross-section (RCS) and two-way propagation of the way by the complex coefficient α_0. Hereafter, we incorporate all constant terms of signal processing into α_0 with no loss of generality. The signal impinging the receiver becomes

$$\begin{aligned} s_r(t) &= \alpha_0 s_t(t - \tau_0(t)) \\ &= \alpha_0 m\left(\left(1 - \frac{2v_0}{c}\right)t - \tau_0\right)e^{-j2\pi f_c\left(1-\frac{2v_0}{c}\right)t} \\ &\quad \cdot e^{j2\pi f_c \tau_0} e^{-j2\pi\frac{\beta}{2}\left(t\left(1-\frac{2v_0}{c}\right)-\tau_0\right)^2} \\ &\approx \alpha_0 m(t - \tau_0) \cdot e^{-j2\pi\left(f_c t - f_D t + \frac{\beta}{2}(t^2 - 2t\tau_0)\right)} \end{aligned} \tag{3}$$

where $f_D = 2v_0 f_c/c$, the constant phase terms are substituted into α_0 and we used $(1 - 2v_0/c) \approx 1$ considering that the velocities typical of automotive scenarios satisfy $v_0 \ll c$. Applying the stretch processing on receive, which consists of multiplication of the received signal with the transmitted chirp and filtering out high-frequency components, results in

$$\begin{aligned} s(t) &= s_r(t)e^{j2\pi\left(f_c t+\frac{\beta t^2}{2}\right)} \\ &= \alpha_0 m(t - \tau_0)e^{j2\pi(\beta\tau_0 + f_D)t} \\ &\approx \alpha_0 m(t - \tau_0)e^{j2\pi\beta\tau_0 t}. \end{aligned} \tag{4}$$

It comprises two main components: the delayed modulated signal and the beat frequency. The second item is standard for dechirping of LFM signals. It also comprises Doppler frequency shift due to target motion, which is typically negligible compared to the frequency resolution of the beat signal after applying FFT to it, i.e., $f_D \ll f_s/N$, where f_s is the sampling frequency of the beat signal and N is the number of fast-time samples.

B. Signal Processing-Filter Bank

The form of (4) can be alternatively interpreted if we denote $f_{\mathrm{VD}} = \beta\tau_0$ as a virtual Doppler frequency shift, which is significantly (about two orders of magnitude) larger than the typical Doppler frequency shift for automotive radars f_D in (4). In this formulation, it resembles a conventional response of a waveform $m(t)$ with the time delay τ_0 and the Doppler frequency shift f_{VD}. This representation is similar to the reception of a general waveform $m(t)$ with a large Doppler shift. In this case, the optimal receiver in white noise is a matched filter for each range-Doppler hypothesis [20]. It can be realized either via a search over all possible range-Doppler bins or via performing Doppler processing prior to range compression. Due to the explicit relation between the parameters $f_{\mathrm{VD}} = \beta\tau_0$, a 1-D search is needed on the parameter τ. Thus, the receiver calculates for each τ

$$y(\tau) = \int s(t)m^*(t - \tau)e^{-j2\pi\beta\tau t}dt. \tag{5}$$

Modern radars perform baseband signal processing digitally, after the received beat signal is sampled by ADC at the sampling frequency f_s and stored in vector $\mathbf{s} \in \mathbb{C}^{N\times 1}$

$$\mathbf{s} = \alpha_0 m(n/f_s - \tau_0)e^{j2\pi\beta\tau_0 n/f_s} \tag{6}$$

where $t = n/f_s, n = 0, \ldots, N-1$.

The reference signal in the integral (5) for the fixed τ can be given via a Hadamard product of two vectors $\mathbf{a}(\tau) \odot \mathbf{m}(\tau)$

$$\begin{aligned} \mathbf{a}(\tau) &= e^{j2\pi\beta\tau n/f_s} \\ \mathbf{m}(\tau) &= m(n/f_s - \tau) \end{aligned} \tag{7}$$

$n = 0, \ldots, N-1$; $\mathbf{a}(\tau), \mathbf{m}(\tau) \in \mathbb{C}^{N\times 1}$.

Stacking the steering vectors of the beat signal and the delayed modulation signal as columns in matrices $\mathbf{A} = [\mathbf{a}(\tau_0), \ldots, \mathbf{a}(\tau_{N_r})]$ and $\mathbf{M} = [\mathbf{m}(\tau_0), \ldots, \mathbf{m}(\tau_{N_r})]$ respectively, with N_r being the predefined number of range cells, it is possible to write the convolution (5) via a vector product

$$\mathbf{y} = (\mathbf{A} \odot \mathbf{M})^H \mathbf{s}. \tag{8}$$

This receiver structure has previously been proposed in [5] and [6] and is called compensated stretch processing. The compensation referred to in the name of the algorithm realizes the proper shift of the reference modulation signal for each

range hypothesis, realized here via matrix **M**. Filter bank realization of compensated stretch processing leads to the computational complexity of DFT $\mathcal{O}(N^2)$.

C. Waveform Analysis and Design

The key block of the receiver (5) [or its digital counterpart (8)] correlates the received signal with the time delay and frequency-shifted template. This is equivalent to calculating the cross correlation of $s(t)$ and $m(t)$ along the diagonal line in the time delay/Doppler shift domain. If we further expand (5), considering the target Doppler frequency shift as in (4), we get

$$\begin{aligned} y(\tau) &= \alpha_0 \int m(t-\tau_0)m^*(t-\tau)e^{-j2\pi(\beta(\tau-\tau_0)-f_D)t}dt \\ &= \alpha_0 \int m(t')m^*(t'-\Delta_\tau)e^{-j2\pi(\beta\Delta_\tau-f_D)t'}dt' \\ &= \alpha_0 \chi_m(\Delta_\tau, -(\beta\Delta_\tau - f_D)) \end{aligned} \tag{9}$$

where $t' = t - \tau_0$, $\Delta_\tau = \tau - \tau_0$ and $\chi_m(\tau, f_D)$ defines the ambiguity function of the waveform $m(t)$; the constant phase term $e^{-j2\pi(\beta\Delta_\tau - f_D)\tau_0}$ was substituted into α with no loss of generality. It implies that the range response of the proposed processing is determined by the diagonal cut of the ambiguity function $\chi_m(\tau, f_D)$. This can be alternatively interpreted as a shear of the ambiguity function of the waveform $m(t)$ being modulated by a chirp [21]. Another consequence of (9) is that the (phase) modulation schemes, optimized for low-range sidelobes, e.g., Barker, Frank, or Zadoff-Chu phase codes [21], would not preserve this property if they are used to modulate a chirp (1). The design of optimal modulation schemes to be applied to the proposed receiver structure is the subject of ongoing research.

III. Fractional Correlation Receiver

In conventional radar signal processing, the time delay (range) and signal frequency shift (Doppler) are typically estimated separately and independent of each other: range via the correlation of the received signal with the replica and Doppler frequency via Fourier transform over slow time—both with a computational complexity of FFT. The former exploits the fact that correlation in time transforms into a simple multiplication operation in the frequency domain [22]

$$\begin{aligned} s(t) \circledast m^*(t-\tau) &= \int s(t)m^*(t-\tau)dt \\ &= \mathcal{F}^{-\frac{\pi}{2}}\{S(f)M^*(f)\} \end{aligned} \tag{10}$$

where $\circledast$ denotes correlation, $\mathcal{F}^{-(\pi/2)}\{\cdot\}$ is the inverse Fourier transform (the reason for this superscript will be explained shortly); $S(f)$ and $M(f)$ are the Fourier transforms of $s(t)$ and $m(t)$, respectively.

Therefore, the objective is to develop an efficient algorithm to calculate the cross correlation along the diagonal line in the time delay/Doppler frequency shift domain (5) with the computational complexity of FFT. This can be done using the theory of FrFT and fractional correlation [23], [24]. Recently FrFT has been widely used in numerous signal processing applications [17], [25], including radar, where it has been applied to focus (inverse) synthetic aperture radar [(I)SAR] images [18], passive radar signal processing [25], coherent integration of moving target over long time intervals [26] and waveform design [27].

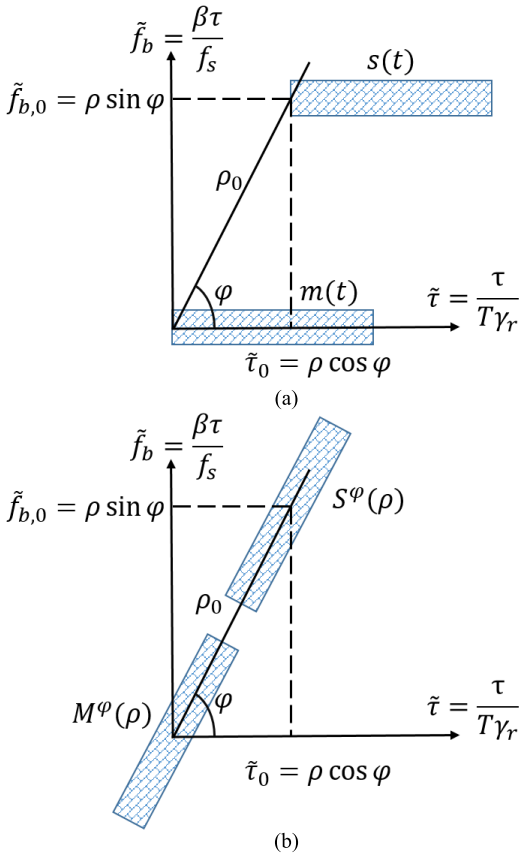

Fig. 1. Time–frequency representation of the received signal and its relation to the FrFT angle φ: (a) before FrFT and (b) after FrFT.

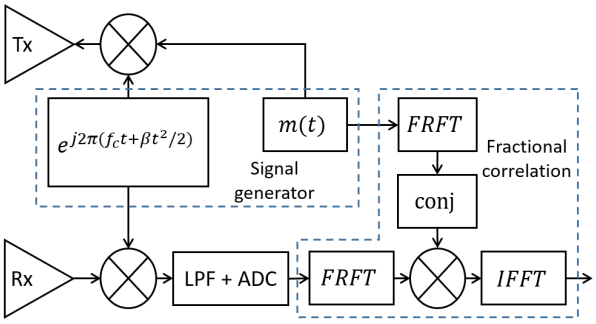

Fig. 2. FRFT receiver structure for modulated FMCW waveforms.

With the use of FrFT, the definition (10) can be extended to calculate the cross correlation along any line in the Doppler-delay plane [24]

$$\begin{aligned} y(\tau) &= s(t) \circledast^{\varphi} m^*(t-\tau) \\ &= \mathcal{F}^{-\frac{\pi}{2}}\left\{S^{\frac{\pi}{2}+\varphi}(\rho)\left(M^{\frac{\pi}{2}+\varphi}(\rho)\right)^*\right\} \end{aligned} \tag{11}$$

where the operators $\circledast^{\varphi}$ and $\mathcal{F}^{\varphi}\{\cdot\}$ denotes fractional correlation and the FrFT associated with angle φ, measured

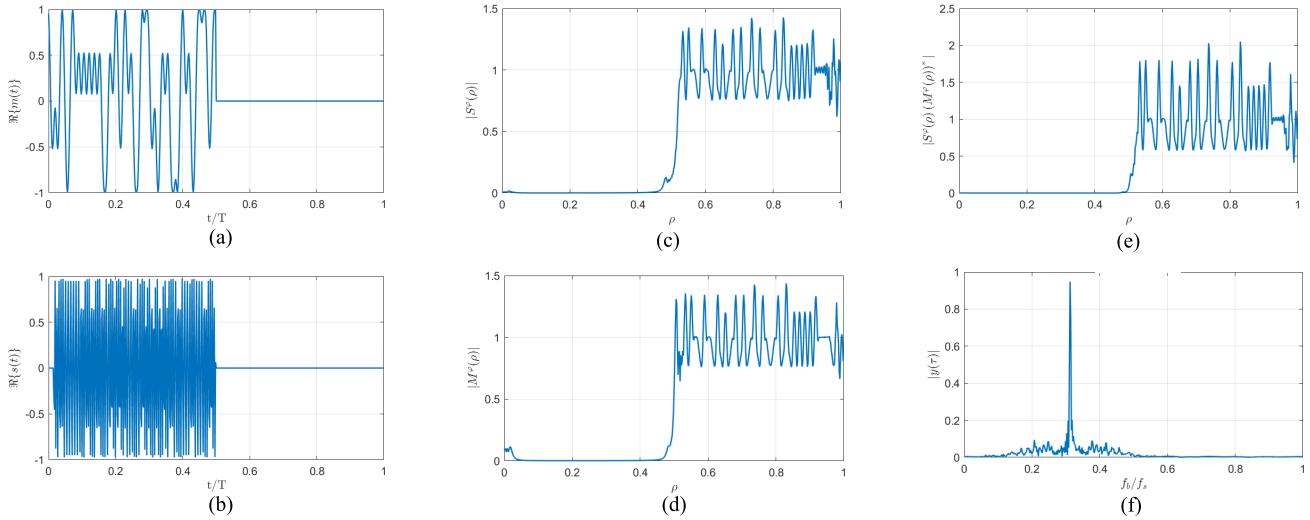

Fig. 3. (a) GMSK modulation signal (real part) $\Re\{m(t)\}$. (b) Received signal (real part) $\Re\{s(t)\}$. (c) FrFT of the modulation signal $M^{(\pi/2)+\phi}(\rho)$. (d) FrFT of the received signal $S^{\frac{\pi}{2}+\phi}(\rho)$. (e) Product of FrFTs $S^{(\pi/2)+\varphi}(\rho)(M^{(\pi/2)+\varphi}(\rho))^*$. (f) Range profile as the result of fractional correlation (11).

anti-clockwise from the time axis, such that $\mathcal{F}^{(\pi/2)}\{\cdot\}$ and $\mathcal{F}^{-(\pi/2)}\{\cdot\}$ correspond to the Fourier transform and inverse Fourier transform, respectively. Moreover, we denote by $S^{\varphi}(\rho) = \mathcal{F}^{\varphi}\{s(t)\}$ and $M^{\varphi}(\rho) = \mathcal{F}^{\varphi}\{m(t)\}$ the φth FrFT (FrFT) of $s(t)$ and $m(t)$ [17], [18], [23] and ρ is the argument in this FrFT domain.

The FrFT of $s(t)$ is defined for angle φ as [24, eq. (9)]

$$S^{\varphi}(\rho) = \sqrt{1 - j\cot\varphi}\, e^{j\pi\rho^2\cot\varphi} \cdot \int s(t) e^{j\pi t^2\cot\varphi - j2\pi t\rho\csc\varphi} dt. \quad (12)$$

The time–frequency representation of the modulation signal $m(t)$ and that of the received signal (4) are presented in Fig. 1 before (a) and after (b) applying FrFT to them. It can be seen that the target range information is fully described by the radial displacement ρ at the angle φ. It was shown in [24, eq. (21)] that the displacement of the signal time–frequency representation by ρ, φ in polar coordinated corresponds to

$$S^{\varphi}(\rho - \rho_0) = \mathcal{F}^{\varphi}\{\tilde{\alpha} s(t - \rho_0\cos\varphi) e^{j2\pi t\rho_0\sin\varphi}\} \quad (13)$$

where we used the notation $\tilde{\alpha} = e^{-j2\pi(\rho_0^2/2)\cos\varphi\sin\varphi}$, as for the FrFT of $s(t)$ [and of $m(t)$] it can be substituted into the constant term of the received signal α_0 with no loss of generality. Given the property (13) of FrFT and comparing it to (4), the relation of the FrFT parameters to the waveform and radar parameters can be found by

$$\begin{cases} \rho_0\cos\varphi = \dfrac{\tau_0}{T\gamma_r} \\ \rho_0\sin\varphi = \dfrac{\beta\tau_0}{f_s} \end{cases} \quad (14)$$

where γ_r is the oversampling factor for range processing. It should also be noted that depending on the sign of the analytical signal in (1) and also on the choice of up/down chirp, the beat frequency can have a negative sign. That should be taken into account at the output of in-phase and quadrature (IQ) demodulation. Furthermore, the angle of FrFT is fully determined by the parameters of the radar according to the ratio of scales in relative frequency shift ($\beta\tau_0/f_s$) to a relative time delay of the signal (τ_0/T) and thus

$$\varphi = \arctan\left(\frac{B\gamma_r}{f_s}\right). \quad (15)$$

The target range depends linearly on the parameter ρ_0

$$\rho_0 = \frac{\tau_0}{T\gamma_r\cos(\arctan\varphi)} = \frac{\sqrt{\varphi^2+1}}{T\gamma_r}\tau_0 \quad (16)$$

and can be directly scaled to the range axis.

The structure of the FrFT receiver is presented in Fig. 2. The key component of the receiver is the fractional correlation block, which is reflected in (11).

It is assumed that the fractional correlation block operates with the sampled signals. The discrete version of FrFT (12) can be derived from the discrete Fourier transform by eigenvalue decomposition of the transformation matrix [17], [28] and maintain most of the properties of continuous FrFT. It approximates well the continuous FrFT for a large number of samples. Ozaktas et al. [19] proposed a faster way to compute an approximation of the continuous fractional Fourier. It exploits the fact that FrFT can be rewritten via a convolution in between two chirp multiplications, which need to be sampled at twice the original sampling rate. The computational complexity of such implementation is $\mathcal{O}(N\log_2 N)$, being determined by the realization of the convolution via FFT [19], [28]. The low computational load and high accuracy made this algorithm a common tool in digital signal processing [17].

It should be noted that the digital calculation of FrFT assumed that the signal is approximately confined to the interval $[-T/2, T/2]$ in time and to the interval $[-f_s/2, f_s/2]$ in frequency. Although the former is easy to satisfy by shifting the time axes of the Rx signal $s(t)$ and the replica $m(t)$ by $-T/2$, breaking the latter assumption results in folding the

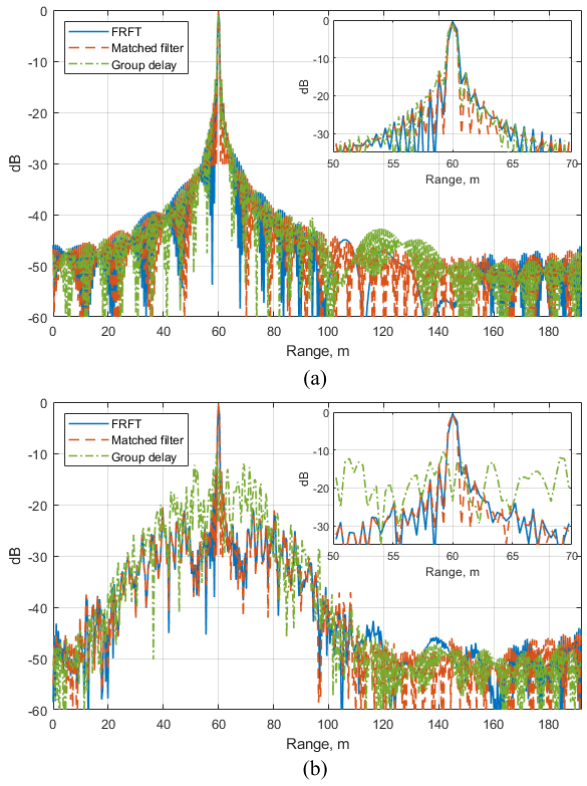

Fig. 4. Estimated range profile of a point-like target with three receiver structures considered: (a) narrowband modulation, $B_m/f_s = 1/64$ and (b) wide-band modulation, $B_m/f_s = 1/4$.

signal in FrFT domain for $f_b > f_s/2$. To avoid frequency folding, we propose to transmit the modulated signal $m(t)$ with a frequency offset $\Delta_f = -f_s/2 + B_m/2$, where B_m is the bandwidth of modulation sequence, which ensures that the sampled received signal is a time–frequency shifted version of the reference one for ranges

$$r \in \left[0, \frac{(f_s - B_m)T}{\Delta_r}\right] \tag{17}$$

where $\Delta_r = c/(2B)$. This criteria for the maximum range is defined assuming that for proper correlation the spectrum of the modulation signal defined by B_m should fall below the cut-off frequency of the low-pass filter (LPF) before ADC. Targets at longer ranges can still be observed, but they will have a larger SNR loss and a significant distortion of the range profile. Modulation of FMCW, therefore, leads to the degradation of the maximum detectable range by the factor $(f_s - B_m)/f_s$. Note that the discussion above assumes the IQ receiver structure; if sampling only the I channel, both signals should belong to the interval $[0, f_s/2]$, and thus the frequency offset should be set to $\Delta_f = B_m/2$.

IV. Simulations

Consider the waveform with chirp bandwidth $B = 200$ MHz, chirp duration $T = 12.8$ μs operating at carrier $f_c = 77$ GHz, and the sampling frequency of the beat signal is $f_s = 20$ MHz. With this setup, the maximum range of FMCW is $R_{\max} = 192$ m. The signal $m(t)$ is the Gaussian

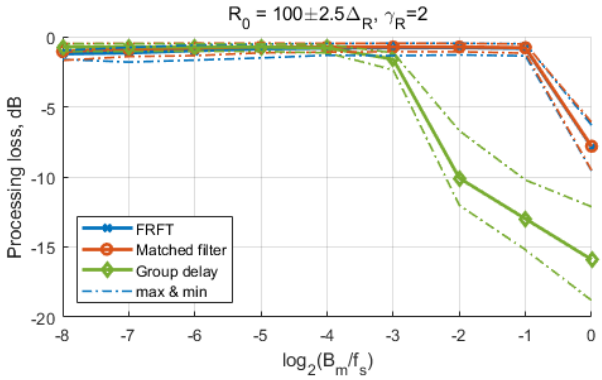

Fig. 5. Processing loss versus the normalized bandwidth of the modulation signal $m(t)$.

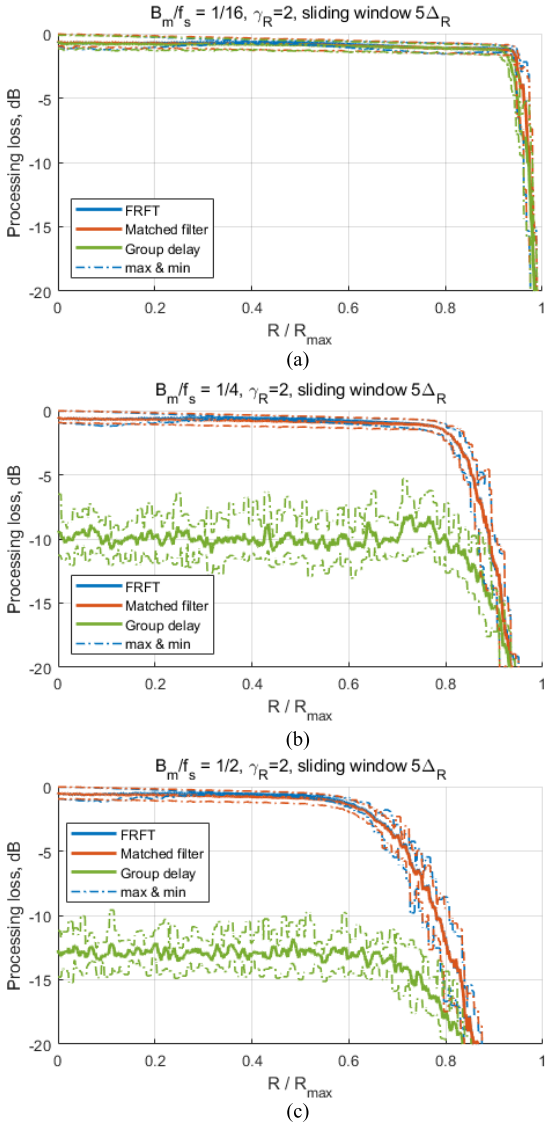

Fig. 6. Processing loss as a function of the target range: (a) narrowband modulation, $B_m/f_s = 1/16$; (b) wide-band modulation, $B_m/f_s = 1/4$; and (c) $B_m/f_s = 1/2$.

minimum shift keying (GMSK) modulated waveform with the time-bandwidth product of GMSK equal to 0.3 [29] and $N = 64$ chips, which corresponds to the modulation signal

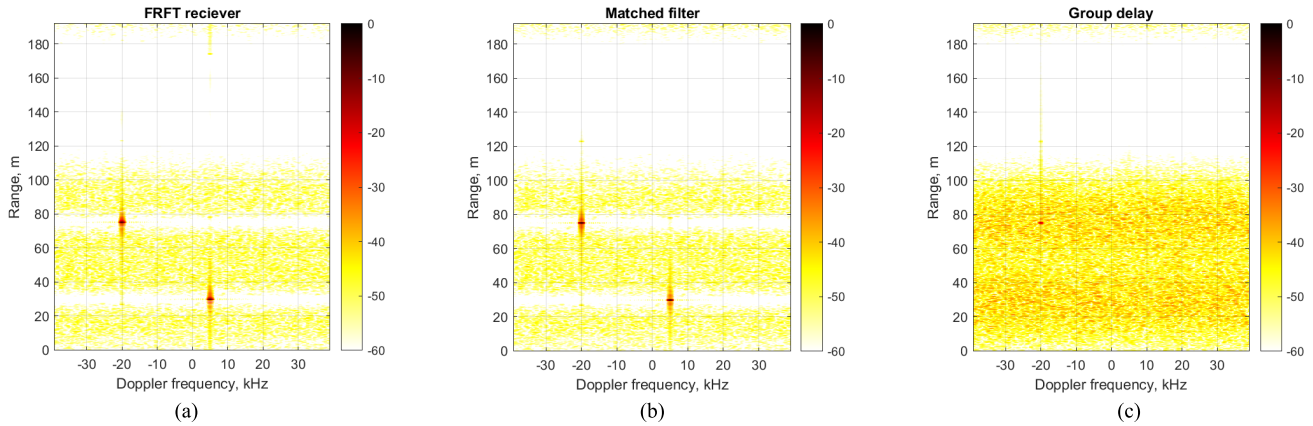

Fig. 7. Range-Doppler processing: (a) FRFT receiver, (b) matched filter bank, and (c) group delay receiver.

bandwidth of $B_m = f_s/4 = 5$ MHz. For range processing, we consider range oversampling $\gamma_r = 2$, which according to (15) gives $\varphi = \arctan(20) \approx 1.52$. To demonstrate the principle of the FrFT receiver, we assume a noise-free scenario with a single stationary point-like target at the range $r_0 = 60$ m from the radar.

A. Principles of FRFT Receiver

The signal representations at all the stages of the fractional correlation (11) are plotted in Fig. 3. Here, we did not apply the frequency shift of the modulation signal, described at the end of the previous section, for better visibility (there is no difference in applying this shift or not for a target at $r_0 \leq R_{\max}/2$). It can be seen that despite the time and frequency shift between the received $s(t)$ and the reference $m(t)$ signals [see Fig. 3(a) and (b)], it vanishes in their FrFT representations [see Fig. 3(c) and (d)]. As a result, their product has a wide and uniform spectrum [see Fig. 3(e)], which leads to a narrow peak in the reconstructed range profile [see Fig. 3(f)].

We further compare the performance of the FrFT receiver to that of the filter bank approach, described in Section II-B (or compensated stretch processing [5], [6]) and to that of the group delay receiver [7], [9] (see Fig. 4). Simulation results demonstrate that all three receivers have comparable range response for small bandwidth of modulation signal $B_m/f_s = 1/64$ [see Fig. 4(a)], but for larger bandwidth of $m(t)$ the performance of group delay receiver degrades significantly compared to that of the filter bank and FrFT approaches (see Fig. 4(b) shows the result for $B_m/f_s = 1/4$). The performance of FrFT receiver is similar to that of the filter bank, being different only in the implementation and related to its computational complexity, as we mentioned above.

B. Processing Loss

To better demonstrate the limit of applicability of the group delay receiver, we compare in Fig. 5 the processing loss as the function of the code bandwidth B_m/f_s normalized by f_s. Similar to the above, we considered a noise-free scenario with a single target present in the scene in the range $r_0 = 60 + w_r$ m, where $w_r \in [-2.5\Delta_r, 2.5\Delta_r]$, models an offset from the defined range grid with a step $0.125\Delta_r$. The plots in Fig. 5 show the average (solid line), the best-case and the worst case (dashed lines) processing loss for three considered receivers. It comprises the attenuation of the signal by the LPF prior to ADC and straddle loss: the mean value indicates the loss due to filtering of the received signal band by LPF prior to ADC sampling in the stretch processing architecture. The gap between lower and upper limits shows the bounds of the straddle loss, that can occur due to off-grid sampling. It can be seen that all three receivers behave similarly for a small code bandwidth: the straddle loss is about 1 dB [30]. For large code bandwidth $B_m/f_s \geq 1/8$, the degradation of the matched filter and the FrFT receiver is dominated by the straddle loss, while the group delay filter leads to a significant (over 10 dB) processing loss, which is also seen via defocusing of the main lobe of the range response in Fig. 4(b). This performance degradation of the group delay receiver for large bandwidth of the modulation signal $m(t)$, previously mentioned in [9], imposes an additional constraint on the choice of the modulation sequence $m(t)$. Finally, it should be noticed that for $B_m/f_s = 1$ all the receivers have degraded performance for observing the target at $r_0 \approx 60$, because a part of the modulated signal spectrum is being rejected by the LPF of the receiver.

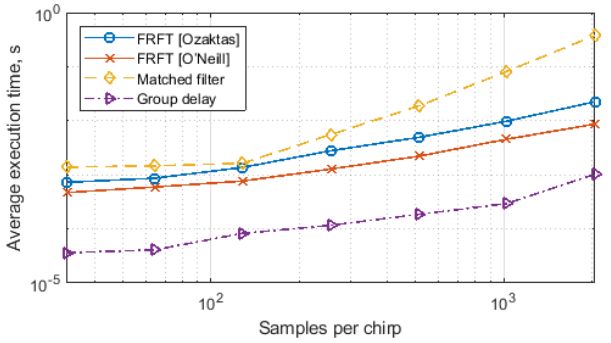

Fig. 8. Computational complexity of three considered receiver structures.

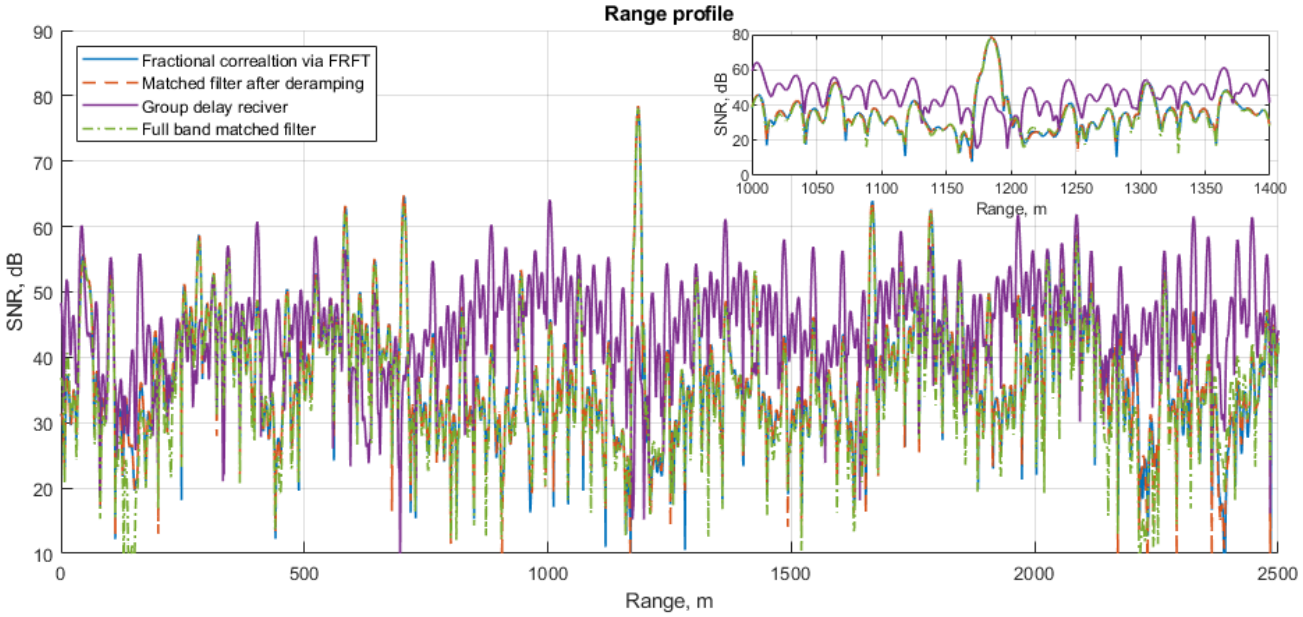

Fig. 9. Measured range profile of a chimney at $r \approx 1185$ m, illuminated by a BPSK modulated chirp.

The bandwidth of the modulation signal has an impact on the maximum detectable target range. We investigate this behavior via simulations in Fig. 6 for three values of the normalized bandwidth of the modulation signal: $B_m/f_s = 1/16$ [see Fig. 6(a)], $B_m/f_s = 1/4$ [see Fig. 6(b)] and $B_m/f_s = 1/2$ [see Fig. 6(c)]. The range axes in Fig. 6 are similar to that in Fig. 4, up to the normalization by a scalar $R_{\max}$. It can be seen, that a small bandwidth of the modulation B_m [see Fig. 6(a)] has almost no impact on the maximum detectable range of the target, while in the case of a significant modulation bandwidth B_m, processing loss rapidly increases for $r \geq 0.8\ R_{\max}$ when $B_m/f_s = 1/4$ and for $r \geq 0.6\ R_{\max}$ when $B_m/f_s = 1/2$. These values slightly exceed the criteria defined in (17), while the latter still gives a reasonable estimation of the maximum range for applying dechirping receiver with a modulated LFM waveform.

C. Range-Doppler Processing

We further demonstrate the performance of the proposed receiver by comparing range-Doppler images of three receiver structures, presented above. For this simulation, we assume the radar transmits $M = 128$ chirps with the parameters, mentioned above and pulse repetition interval (PRI) $T_r = T$. Each chirp is modulated with a different random GMSK modulation with $B_m = f_s/4 = 5$ MHz. Two targets resulting in equal Rx power are present in the scene: $r_0 = 60$ m and Doppler frequency $f_{D,0} = 5$ kHz; $r_1 = 75$ m $f_{D,1} = -20$ kHz. The proposed processing is applied per chirp, followed by a Doppler FFT with Hamming window to reduce Doppler sidelobes. Range-Doppler maps of the FRFT receiver, the matched filter bank and the group delay receiver are demonstrated in Fig. 7(a)–(c), respectively. The FRFT receiver and the matched filter bank indicate the responses of both targets at their correct positions and provide about 50 dB dynamic range [21 dB slow-time gain and about 30 dB per chirp, see Fig. 4(b)], which significantly outperforms the group delay receiver.

D. Computational Complexity

Further, we compared the average over 100 trials execution time of each of the three receivers (for a single chirp) as the function of fast-time samples per chirp (see Fig. 8). In this simulation, we used two different implementations of FrFT: `fracF`–the direct implementation of algorithm [19] in MATLAB by Ozaktas et al. and `fracFT`–the implementation of FrFT [19] by O'Neill [31]. The difference between these implementations is discussed in detail in [28].

The results in Fig. 8 show that the slope of the FrFT and group delay receivers follows the trend $\mathcal{O}(N \log_2(N))$ and the complexity of the matched filter increases according to $\mathcal{O}(N^2)$. Two implementations of FrFT have slightly different execution time: the one by O'Neill [31] being more efficient. For a moderate to a large number of samples per chirp, the FrFR receiver has a gain of more than one order of magnitude in computational time. The group delay receiver reduces the execution time even more, but its performance for long code sequences is unsatisfactory, as explained above.

V. Experimental Validation

The experimental validation of the proposed processing technique was performed with polarimetric agile radar in S band (PARSAX) radar [32], installed on the rooftop of 100 m high electrical engineering, mathematics, and computer science (EEMCS) building of the Delft University of Technology. The radar was pointing to the top of an industrial chimney, located about 1185 m away from the radar. A single (HH) polarimetric channel was used for the measurements. The waveforms settings are: $f_c = 3.315$ GHz, $B = 40$ MHz, $T_r \approx 1$ ms; $m(t)$ is a binary phase shift keying (BPSK) sequence with $B_m \approx 1$ MHz. The raw data was collected

at the intermediate frequency $f_{\mathrm{IF}} = 125$ MHz, followed by the downconversion to the baseband, deramping (this and the following steps are not applied for the full band matched filter processing, considered below), downsampling to $f_s \approx 4.2$ MHz (corresponding to 4096 range cells), and applying one of the considered range processing techniques. Chebyshev windowing with 80 dB sidelobe level and range oversampling with $\gamma_r = 4$ are applied for all the techniques [for the IFFT in (11)]. The results demonstrated in Fig. 9 compare the performance of the fractional correlator (11), matched filter bank after deramping (8), group delay receiver [9] and the matched filtering in the full band. The results demonstrate that the group delay filter performs poorly with the selected bandwidth of the code, while the other techniques demonstrate similar performance. This comes with the high sampling rate requirements of the full-band matched filtering and low computational efficiency of the matched filter bank after deramping (8). The proposed fractional correlator obtains the same result with low ADC sampling and computational complexity requirements.

VI. Conclusion

In this article, we proposed the new receiver structure for the modulated LFM waveform, which can be realized in simple hardware and requires computational resources similar to FFT. We demonstrated that matched filter processing of this waveform corresponds to calculating the cross correlation along a diagonal line in the delay-Doppler plane-called Fractional correlation, which can be efficiently implemented via the FrFT. The receiver, based on the proposed principle, offers a significant improvement over the state-of-the-art techniques for moderate-to-large bandwidths of modulation signals, as demonstrated via numerical simulations and experimental processing from waveform-agile radar PARSAX.

Acknowledgment

The authors would like to thank Utku Kumbul and Fred van der Zwan for conducting the measurements and sharing the experimental data. The research has been performed and the article was written while both authors were with the Microwave Sensing, Signals and Systems (MS3) Section, Faculty of Electrical Engineering, Mathematics, and Computer Science (EEMCS), Delft University of Technology.

References

[1] H. Sun, F. Brigui, and M. Lesturgie, "Analysis and comparison of MIMO radar waveforms," in *Proc. Int. Radar Conf.*, Oct. 2014, pp. 1–6.

[2] J. J. M. De Wit, W. L. Van Rossum, and A. J. De Jong, "Orthogonal waveforms for FMCW MIMO radar," in *Proc. IEEE RadarCon (RADAR)*, Kansas City, MO, USA, May 2011, p. 686.

[3] J. Reneau and R. R. Adhami, "Phase-coded LFMCW waveform analysis for short range measurement applications," in *Proc. IEEE Aerosp. Conf.*, Mar. 2014, pp. 1–6.

[4] M. Nowak, M. Wicks, Z. Zhang, and Z. Wu, "Co-designed radar-communication using linear frequency modulation waveform," *IEEE Aerosp. Electron. Syst. Mag.*, vol. 31, no. 10, pp. 28–35, Oct. 2016.

[5] P. M. McCormick, C. Sahin, S. D. Blunt, and J. G. Metcalf, "FMCW implementation of phase-attached radar-communications (PARC)," in *Proc. IEEE Radar Conf. (RadarConf)*, Apr. 2019, pp. 1–6.

[6] D. M. Hemmingsen et al., "Waveform-diverse stretch processing," in *Proc. IEEE Radar Conf. (RadarConf)*, Apr. 2018, pp. 963–968.

[7] F. Uysal, "Phase-coded FMCW automotive radar: System design and interference mitigation," *IEEE Trans. Veh. Technol.*, vol. 69, no. 1, pp. 270–281, Jan. 2019.

[8] F. Uysal, "Phase coded frequency modulated continuous wave (FMCW) radar system," U.S. patent NL2020050066 W, Feb. 8, 2019.

[9] F. Lampel, R. F. Tigrek, A. Alvarado, and F. M. Willems, "A performance enhancement technique for a joint FMCW radcom system," in *Proc. 16th Eur. Radar Conf. (EuRAD)*, 2019, pp. 169–172.

[10] F. G. Jansen, F. Laghezza, and F. Lampel, "Radar-based communication," U.S. patent US2020256948 A1, Aug. 13, 2020.

[11] A. Meta, P. Hoogeboom, and L. P. Ligthart, "Signal processing for FMCW SAR," *IEEE Trans. Geosci. Remote Sens.*, vol. 45, no. 11, pp. 3519–3532, Oct. 2007.

[12] H. Krichene, E. Brawley, K. Lauritzen, A. Wu, and S. Talisa, "Time sidelobe correction of hardware errors in stretch processing," *IEEE Trans. Aerosp. Electron. Syst.*, vol. 48, no. 1, pp. 637–647, Jan. 2012.

[13] Y. X. Zhang, R.-J. Hong, P.-P. Pan, Z.-M. Deng, and Q.-F. Liu, "Frequency-domain range sidelobe correction in stretch processing for wideband LFM radars," *IEEE Trans. Aerosp. Electron. Syst.*, vol. 53, no. 1, pp. 111–121, Feb. 2017.

[14] F. Laghezza and F. Lampel, "Predistortion technique for joint radar/communication systems," U.S. patent EP3907520 A1, Nov. 4, 2021.

[15] U. Kumbul, N. Petrov, C. S. Vaucher, and A. Yarovoy, "Smoothed phase-coded FMCW: Waveform properties and transceiver architecture," *IEEE Trans. Aerosp. Electron. Syst.*, 2022, *arXiv:2203.07508*.

[16] D. Schindler, B. Schweizer, C. Knill, J. Hasch, and C. Waldschmidt, "MIMO-OFDM radar using a linear frequency modulated carrier to reduce sampling requirements," *IEEE Trans. Microw. Theory Techn.*, vol. 66, no. 7, pp. 3511–3520, Jul. 2018.

[17] R. Tao, B. Deng, and Y. Wang, "Research progress of the fractional Fourier transform in signal processing," *Sci. China F*, vol. 49, no. 1, pp. 1–25, Jan. 2006.

[18] Z. Xinghao and T. Ran, "The new algorithm for passive radar MTD based on the fractional correlation," in *Proc. 7th Int. Conf. Signal Process.*, vol. 3, Aug. 2004, pp. 2061–2065.

[19] H. M. Ozaktas, O. Arikan, M. A. Kutay, and G. Bozdagt, "Digital computation of the fractional Fourier transform," *IEEE Trans. Signal Process.*, vol. 44, no. 9, pp. 2141–2150, Sep. 1996.

[20] M. I. Skolnik, *Radar Handbook*. New York, NY, USA: McGraw-Hill, 2008.

[21] N. Levanon and E. Mozeson, *Radar signals*. Hoboken, NJ, USA: Wiley, 2004.

[22] S. W. Smith et al., *The Scientist and Engineer's Guide to Digital Signal Processing*. San Diego, CA, USA: California Technical, 1997.

[23] L. B. Almeida, "The fractional Fourier transform and time-frequency representations," *IEEE Trans. Signal Process.*, vol. 42, no. 11, pp. 3084–3091, Nov. 1994.

[24] O. Akay and G. F. Boudreaux-Bartels, "Fractional convolution and correlation via operator methods and an application to detection of linear FM signals," *IEEE Trans. Signal Process.*, vol. 49, no. 5, pp. 979–993, May 2001.

[25] E. Sejdić, I. Djurović, and L. Stanković, "Fractional Fourier transform as a signal processing tool: An overview of recent developments," *Signal Process.*, vol. 91, no. 6, pp. 1351–1369, Jun. 2011.

[26] X. Chen, J. Guan, N. Liu, and Y. He, "Maneuvering target detection via radon-fractional Fourier transform-based long-time coherent integration," *IEEE Trans. Signal Process.*, vol. 62, no. 4, pp. 939–953, Feb. 2014.

[27] D. Gaglione et al., "Waveform design for communicating radar systems using fractional Fourier transform," *Digital Signal Processing*, vol. 80, pp. 57–69, 2018.

[28] A. Bultheel and H. E. M. Sulbaran, "Computation of the fractional Fourier transform," *Appl. Comput. Harmon. Anal.*, vol. 16, no. 3, pp. 182–202, May 2004.

[29] J. B. Anderson, T. Aulin, and C.-E. Sundberg, *Digital Phase Modulation*. New York, NY, USA: Springer, 2013.

[30] M. A. Richards, J. Scheer, W. A. Holm, and W. L. Melvin, *Principles of Modern Radar*. Edison, NJ, USA: SciTech, 2010.

[31] J. C. O'Neill. (2012). *Discrete TFDs: Time-Frequency Analysis Software*. [Online]. Available: http://tfd.sourceforge.net/

[32] O. A. Krasnov, L. P. Ligthart, Z. Li, G. Babur, Z. Wang, and F. Van Der Zwan, "PARSAX: High-resolution Doppler-polarimetric FMCW radar with dual-orthogonal signals," in *Proc. 18th Int. Conf. Microw., Radar Wireless Commun.*, 2010, pp. 1–5.

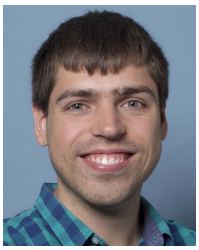

Nikita Petrov received the B.Eng. degree in radio-electronic control systems from Baltic State Technical University "Voenmeh," Saint Petersburg, Russia, in 2012, and the Ph.D. degree in radar signal processing from the Delft University of Technology, Delft, The Netherlands, in 2019.

Since 2019, he has been a Post-Doctoral Researcher with the Microwave Sensing, Signals and Systems (MS3) Section, Faculty of Electrical Engineering, Mathematics, and Computer Science (EEMCS), Delft University of Technology. Since April 2022, he has been with NXP Semiconductors, Eindhoven, The Netherlands and part time with the same university at the Delft University of Technology. His research interests include modern radar technologies, radar signal processing, multichannel and multiband signals and systems, and high resolution and automotive radars.

Dr. Petrov currently serves as a Reviewer for IEEE TRANSACTIONS ON AEROSPACE AND ELECTRONIC SYSTEMS and IEEE TRANSACTIONS ON GEOSCIENCE AND REMOTE SENSING.

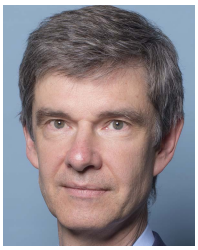

Alexander G. Yarovoy (Fellow, IEEE) received the Diploma degree (Hons.) in radiophysics and electronics, the Candidate of Sciences (Physics and Mathematics) degree in radiophysics, and the Doctor of Sciences (Physics and Mathematics) degree in radiophysics, from Kharkov State University, Kharkiv, Ukraine, in 1984, 1987, and 1994, respectively.

In 1987, he joined the Department of Radiophysics, Kharkov State University, as a Researcher, and became a Full Professor in 1997. From September 1994 to 1996, he was with the Technical University of Ilmenau, Ilmenau, Germany, as a Visiting Researcher. Since 1999, he has been with the Delft University of Technology, Delft, The Netherlands, where he has been leading the Chair of Microwave Sensing, Signals and Systems, since 2009. He has authored and coauthored more than 500 scientific or technical articles, seven patents, and 14 book chapters. His main research interests include high-resolution radar, microwave imaging, and applied electromagnetics (in particular, ultra-wideband (UWB) antennas).

Prof. Yarovoy was a recipient of the European Microwave Week Radar Award for the paper that best advances the state-of-the-art in radar technology in 2001 (together with L. P. Ligthart and P. van Genderen) and in 2012 (together with T. Savelyev). In 2010, together with D. Caratelli, he received the Best Paper Award of the Applied Computational Electromagnetic Society (ACES). He served as the General TPC Chair for the 2020 European Microwave Week (EuMW 2020), the Chair and the TPC Chair for the Fifth European Radar Conference (EuRAD 2008), and the Secretary for the First European Radar Conference (EuRAD 2004). He also served as the Co-Chair and the TPC Chair for the Tenth International Conference on GPR (GPR 2004). He served as an Associate Editor for the *International Journal of Microwave and Wireless Technologies* from 2011 to 2018 and a Guest Editor for five special issues of the IEEE TRANSACTIONS and other journals. From 2008 to 2017, he served as the Director for the European Microwave Association (EuMA).